# Two-dimensional fifth-order Raman spectroscopy of liquid formamide: Experiment and Theory

Y. L. Li,[1] L. Huang,[1] R. J. Dwayne Miller,[1,a)] Taisuke Hasegawa,[2] and Yoshitaka Tanimura[2]
[1]*Departments of Chemistry and Physics and the Institute for Optical Sciences, University of Toronto, 80 St. George Street, Toronto, Ontario M5S3H6, Canada*
[2]*Department of Chemistry, Graduate School of Science, Kyoto University, Sakyoku, Kyoto 606-8502, Japan*

(Received 12 February 2008; accepted 21 April 2008; published online 19 June 2008)

The fifth-order two-dimensional (2D) Raman spectrum of liquid formamide has been obtained. The absolute signal levels, qualitative features, as well as quantitative aspects of the 2D spectrum are found to be in good agreement with recent molecular dynamics calculations. The most important singular feature is the relatively strong rephasing signal observed along the diagonal. This finding illustrates the more structured nature of the hydrogen bond network of liquid formamide in comparison with simple liquids as exemplified by $CS_2$. The theoretical calculations have been extended to include comparisons of different potentials that illustrate the sensitivity of the experiment to the anharmonic motions in the liquid state. The theoretical results point out the key features in the 2D spectrum that probe the essential details in the intermolecular potential. The experiment has been demonstrated to provide new insight into collective effects operating in hydrogen bonded liquids and opens up the exploration of other liquids with this approach.
 [DOI: 10.1063/1.2927311]

## I. INTRODUCTION

One of the most sought after goals in physical chemistry is a detailed microscopic picture of the liquid state. This motivation is driven by the overwhelming fraction of chemistry that occurs in the solution phase. It is now well appreciated that the dynamic response of the solvent along the reaction coordinate plays a major role in defining the reaction pathway.[1–6] The relative motions of molecules in the liquid state require correlated motions over a multitude of length scales that contribute to the rate of passage of a reactive system through a barrier. These motions constitute a manybody problem, in which the underlying intermolecular potential is highly anharmonic.[7–9] On very short time scales, the relative nuclear coordinates appear to be frozen and can be well approximated by an instantaneous modal description,[10–13] although one that is undergoing rapid dephasing. However, as time evolves, initial inertial-like fluctuations in a nominally bound potential lead to changes in nuclear configurations that in turn lead to diffusion. These features to liquid state dynamics enable rapid fluctuations and pair encounters that promote chemical processes. The boundary between inertial type collective motions or modes and diffusive type motions demarcates the onset of liquid behavior. The relative frequency range of these relative intermolecular motions for low viscosity liquids is typically in the frequency range of 10–1000 $cm^{-1}$. The important point is that the relevant motions characterizing the liquid state are highly anharmonic.

This problem is quite challenging from an experimental point of view as the frequency spectrum governing the intermolecular motions of the liquid state is quite congested and lie in a spectral region that is not readily accessible to nonlinear spectroscopic methods. Through recent efforts in terahertz spectroscopy, and depolarized Raman, and time domain equivalents, we now have accurate spectral density of states information on a number of liquids.[14–20] In addition, it is possible to attain atom-pair correlation functions of the liquid state through x-ray and neutron scattering.[21–25] In all cases, the information content is dominated by the harmonic terms in the intermolecular potential. As an example, to first order, the various potentials for liquid water can equally explain the one-dimensional frequency spectrum and the heavy atom-pair correlation function for liquid water.[21] The frequencies and average spatial positions are defined by the harmonic terms in the potential. The key information on the anharmonic terms is not accessed by these experiments. This information can only be accessed by higher order time domain experiments that are capable of directly following anharmonic motions and cancelling out dephasing due to the inhomogeneous distribution in nuclear configurations and associated spectral components.[26–28] Two-dimensional (2D) experiments, in which an additional time correlation is imprinted on the system response that leads to rephasing and cancellation of inhomogeneous dephasing contributions to the signal, are required. This class of experiments is fully capable of determining the homogeneous linewidths that are needed to understand the degree of coupling to the bath (the surrounding molecules with respect to the excited transition) and anharmonic coupling between modes.[29,30] This approach has been used to great effectiveness in the recent development of 2D IR methods[31,32] for observing intramolecular vibrations.[33–39] The problem is that there is no source technology that is sufficiently high power in the terahertz range

a)Author to whom correspondence should be addressed. Electronic mail: dmiller@lphys.chem.utoronto.ca.

 

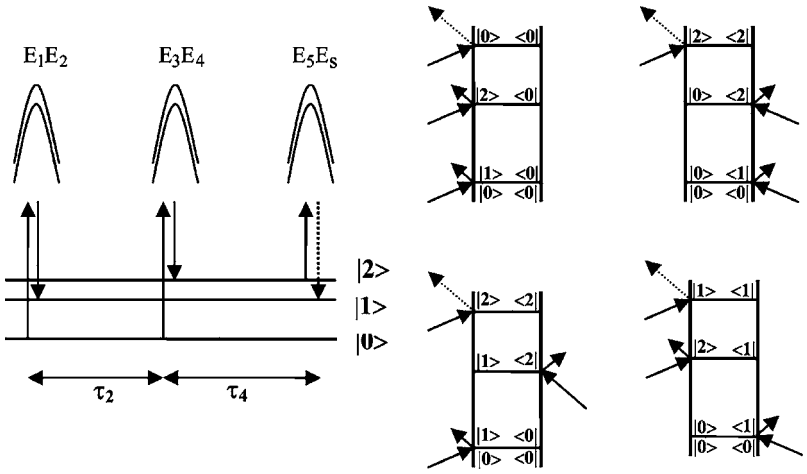


FIG. 1. Energy level and Feynman diagram for fifth-order Raman spectroscopy. The key step responsible for rephasing of the nuclear response and removal of inhomogeneous broadening is the action of the fields at $\tau_2$ that generate a coherence between the ground and Raman overtone, a two-quantum transition, and projects out the anharmonic contributions to the nuclear response.

to enable the direct extension of nonlinear methods to the study of intermolecular motions. The only recourse, at present, is to use Raman scattering to access the intermolecular frequency correlations.[4] From an experimental standpoint, the use of a Raman process is challenging as the field interaction through the coordinate dependent polarizability is much weaker than the direct dipolar coupling to the field as in the case of IR or terahertz spectroscopy. The signal levels are orders of magnitude smaller than the equivalent dipolar coupling term to the field interaction with the same modes.

In this regard, the work of Tanimura and Mukamel was seminal.[27] Prior to this work, it was thought that one needed to conduct a 2D Raman process that is formally equivalent to 2D IR or photon echo experiments, in which the rephasing step of the second pulse acts on the same states. In the photon echo case,[40] this involves a total of four fields, the three input fields, and the generated signal field, such that the experiment is an example of four-wave mixing involving the $\chi^{(3)}$ tensor through the three input fields. A Raman process exciting a given vibration requires a two field interaction through the coordinate dependent polarizability, such that this class of experiments would require a total of eight fields at the $\chi^{(7)}$ level of interaction.[41] The new insight gained from the work of Tanimura and Mukamel was the realization that a rephasing process could be accomplished through an overtone rather than trying to invert the population of the same initially excited levels. This difference reduces the Raman echo experiment to a six-wave mixing process or $\chi^{(5)}$ experiment. This difference greatly reduces the complexity of retaining selective phase matching for a fifth-order experiment over a seventh-order process and the signal levels are correspondingly larger. The different pulse sequences and field interactions are shown in Fig. 1 using energy level and double-sided Feynman diagrams to depict the coherence processes and the evolution of the density matrix along different Liouville space pathways.[27,42,43] In considering these diagrams, the most important point is that rephasing of the coherence induced by the second pair of excitation pulses occurs through a two-quantum or Raman overtone process. Effectively, one needs to drive a given mode hard enough to excite anharmonic terms that introduce spatial components to the nonlinearly induced polarization in the medium.[4] These anharmonic motions are exactly those we wish to observe in order to understand the liquid state.

Since this initial work, there has been a great deal of theoretical work done using the fifth-order Raman process as a benchmark for developing more accurate models of the liquid state.[44–69] The three-point time correlation function of the $q$ (coordinate) dependent polarizability has been shown to be very sensitive to the form of the potential used. Approaches from analytical methods using Brownian oscillators for the bath and mode coupling theory to molecular dynamics (MD) simulations with various model potentials have been employed. Further, the theoretical work has been able to separate the requirements of a nonlinear response in either the electronic polarizability or the anharmonicity of the modes; i.e., the fifth-order signal vanishes unless there is a higher term in the expansion of the induced polarization, $\alpha^{(2)}$, which arises either through nonlinear coupling of the polarization to the field (NL term) or anharmonicity in the potential (AN term).[44–46,55,56] For example, in the case of Xe, the anharmonic coupling term dominates and leads to a focusing of the 2D spectrum along the population waiting time.[55,56] Similarly, this term has been shown to dominate the 2D spectrum of $CS_2$ and other liquids[67] and solids.[68,69] Collectively, the very intensive theoretical work in this area over the past ten years[27,44–69] has shown that the fifth-order Raman response is exquisitely sensitive to the details of the intermolecular potential. Essentially, the modeled experiment provides a direct observation of the anharmonic terms that define the liquid state.

On the experimental front, there has also been a great deal of activity that has led to both significant advances in understanding high order nonlinear spectroscopy and experimental methodology dealing with small signal extraction and phase matching to avoid complicating low order cascades.[4,70–77] The key advances were the introduction of selective phase matching geometries[71,75] that discriminated against lower order cascades and heterodyne detection for small signal amplification.[72,77] The use of heterodyne detection in fifth-order Raman is particularly challenging as it requires phase locking of all six fields. In this regard, the real power of diffractive optics based nonlinear spectroscopy has

been demonstrated.[71,72] Diffractive optics based six-wave mixing provides a single optic approach for encoding the beam geometry for even complex phase matching geometries with excellent contrast against lower order processes and simultaneously provides passive phase stabilization of all of the field interactions.

For the most part, the experimental work has been primarily confined to studies of liquid $CS_2$ that has the highest nonlinear polarizability.[4] Two separate groups have reportedly removed cascaded $\chi^{(3)}$ artifacts through phase matching[75–77] or combinations of phase matching, polarization configurations, pathlength, and phase contrast in heterodyne detection.[4,70–74] The measured fifth-order Raman in these reports shares some similarity in the 2D spectrum with respect to details along the diagonal in terms of rapid loss in bath memory. The most distinctive difference between the two reports was along the coherence time delay or excitation delay ($\tau_2$ nomenclature) for zero population waiting time ($\tau_4=0$) where there should be no $\chi^{(5)}$ nuclear response.[4,70] This signal contribution was assigned to an electronic-nuclear hyperpolarizability term in the $\chi^{(5)}$ response that was potentially different for the one-color experiments[75–77] versus the two-color experiments[70–74] used to reduce scattered light from the excitation pulses in the signal detection. This signal contribution could also equally be explained by residual cascade contributions.[4,70] An important polarization configuration was proposed, in which the two excitation pairs and probe are superimposed with 60° permutations that cancel the lower order $\chi^{(3)}$ response.[63] This polarization configuration has been coined the Dutch Cross[73] and provides an important test for the elimination of lower order cascades from the fifth-order signal and assessment of the signal purity (*vide infra*). This study[73] showed the 2D signal to be focused along the $\tau_2=0$ axis or probe delay with a fast decay in the rephasing ability of the liquid along the diagonal, in agreement with the earlier studies.[70–72] In addition, we recently repeated the studies of liquid $CS_2$ with one-color (800 nm excitation pulse sequences and probe) and find that, as expected based on theoretical grounds, there is no signal along the $\tau_4=0$ axis.[78] These results are identical to our earlier report using the two-color diffractive optic approach.[70–73] The final discrepancy in the experimental results has been resolved by using the Dutch Cross polarization, in which Kaufman *et al.*[79] found that the very large signal along the $\tau_4=0$ axis vanished. The 2D spectrum was in good agreement with previous reports by Kubarych and co-workers.[70–73] It appears that the earlier work of Kaufman *et al.*[77] contained some cascaded $\chi^{(3)}$ contributions in addition to fifth-order Raman signal that would have modified the location of nodal planes in the 2D spectrum and gives rise to the signal along $\tau_2$ ($\tau_4=0$ axis).

The experimental and theoretical results have now converged to a general agreement on the form of the fifth-order Raman response of liquid $CS_2$.[80] This convergence has been solidified with the more recent demonstration of the fifth-order Raman response for liquid benzene.[74] This was the first liquid, in which 2D Raman spectrum has been collected, that was not liquid $CS_2$ and demonstrated the viability of extending this spectroscopy to the study of other liquids.

The above experiments have all treated relatively simple unstructured liquids, in which a modal basis for describing the relative molecular motions is marginally accurate. The ultimate goal in this line of study is to probe the highly correlated motion in more structure liquids, with water being the ultimate goal.[81] Unfortunately, the anisotropic polarizability of water is extremely small. The predicted signal is two orders of magnitude smaller than $CS_2$,[82] such that further advances in experimental methodology are required to achieve this objective. Given the experimental difficulties in executing these experiments, theoretical guidance is needed in which the relative signal strengths can be estimated. The first approach that was capable of making determinations of expected signal levels was the perturbative finite field method of Jansen *et al.*[63] The finite field method avoids having to deal with the enormous memory requirements in generating the stability matrix in equilibrium MD methods; however, it is also plagued by rather large computational requirements in subtracting off lower order field contributions to the response. The computational requirements make it equally difficult to that of the experiment in terms of studying different liquids given the intensive resource requirements. Recently, a hybrid method has been developed that greatly reduces the computation requirements by keeping features of the equilibrium MD methods but avoiding having to compute the stability matrix by using the finite field perturbation to generate the calculated observable.[82] This development has now made it possible to theoretically calculate the expected signal amplitudes for a number of liquids to help direct experimental efforts more efficiently.

The most important prediction from this work was that the fifth-order signal of liquid formamide is only five times smaller than that of liquid $CS_2$.[82] The studies of $CS_2$ have enabled optimization of the experimental parameters, such that there is sufficient signal to noise to enable the study of liquids with this level of $\chi^{(5)}$ response. What is most important is that formamide is a highly hydrogen bonded liquid.[16,83–86] As in the case of water, the highly hydrogen bonded structures rapidly interconvert over some length and time scale. The high degree of correlation imposed by the hydrogen bonds makes this system much more structured than simple liquids. There are important corresponding differences in the predicted 2D Raman spectrum[82] that serve as important tests for the liquid potential used in this calculation and improving our understanding of hydrogen bonded networks. The present study is the first to obtain the fifth-order Raman spectrum of a hydrogen bonded liquid and represents an important step forward in advancing this methodology that arguably provides one the most sensitive probes of the liquid state.

## II. EXPERIMENTAL AND THEORETICAL METHODS

### A. Optical setup

A detailed description of the experimental apparatus has been given elsewhere.[70] The laser system has been updated and only a brief description is provided here. A homebuilt, Kerr-lens mode-locked Ti:sapphire oscillator pumped by a commercial Coherent Verdi (Nd:YVO4) operating at 532 nm

delivers 300 mW output power centered at 800 nm to produce a 100 MHz pulse train of 15 fs seed pulses to a chirped pulse regenerative amplifier. The Ti:sapphire regenerative amplifier is, in turn, pumped by a homebuilt, Q-switched two-head Nd:YLF (yttrium lithium fluoride) which provides 5.5 mJ pulses centered at 527 nm with approximately 1% intensity fluctuations. The resultant, approximately 1 mJ amplified pulses are compressed in a grating compressor to give 0.55 mJ pulses at 1 kHz with a pulse duration of approximately 60 fs. A small fraction of the final output pulse was picked off to serve as the 10 $\mu$J, 800 nm red probe beam, leaving the rest of the beam to be converted to the second harmonic at 400 nm by using a beta barium borate crystal to achieve 0.14 mJ average pulse energies; this blue pulse is further divided down into two equal branches to attain two independent excitation pump pairs. Both the red and blue pulses are compressed by a prism precompressor to reduce the broadening effects caused by the dispersion in the intervening optical elements comprising the diffractive optic setup. Two independent stepper translation stages are separately used to change the relative time delay between the probe beam relative to the first and the second pump beams. Polarizers in transmission mode, half wave plates, and telescopes are set up in three independent arms, leading to one probe and two pump beams focused onto a custom-made diffractive optic (DO) with a 200 $\mu$m spot size.

After the DO, six pulses—two pump laser pairs, one probe pulse, and one reference pulse—with the desired beam geometry for phase matched direct fifth-order Raman signal are imaged onto the sample by two off-axis parabolic mirrors with the conjugate ratio (1.45:1). After the sample, the scattered signal, passing an iris, polarizer, prism, and a focusing lens, is collected by a sensitive photodiode that is fed into a lock-in amplifier (Princeton Applied Research model 5210) in combination with an optical chopper which is used to chop one of the pump laser beams.

There are a number of specific features to this experiment that greatly aid in the alignment and stable signal detection. First and foremost, the reference beam is completely collimated with the scattered signal making it straightforward to find the initial signal and implement heterodyne detection. The DO, without any additional stabilization or vibration isolation, provides better than $\lambda/50$ phase stability in the visible for periods of hours. This feature is extremely important as the signal is very small and requires up to 20 min scans for a single slice in the 2D spectrum. Additional vibration isolation will help future experiments as the slow drift still makes it difficult to collect a 2D spectrum for liquids with such small signals as liquid formamide. In order to avoid the unwanted nonlinear processes in the DO itself from contributing to instability in the signal, different mounts of glasses are inserted in the pulse pairs between the DO and the sample to allow the pulses to arrive at different times in the DO and then made time coincident in the sample. To avoid density fluctuations in the liquid and maintain maximum phase stability, the reference is passed through the same region as the pump and probe beams. This introduces a small pump induced modulation of the reference amplitude. The magnitude of this effect is determined by blocking the pump and collecting a pump induced modulation scan and the signal normalized appropriately with this correction. Similarly, the reference is blocked to collect the homodyne signal and subtracted from the data. Probe induced modulation effects are negligible. The accuracy of the removal of the pump induced modulation of the reference is determined by comparison of the collected homodyne or signal intensity scans along the same time slices, as previously shown.[70] A flowing cell containing spectroscopic grade liquid formamide was used to avoid any possible accumulated photochemistry, although none was observed even after many hours of laser shots. However, the baseline of the signal was found to rise over time due to nonlinear index changes in the windows. This baseline contribution could be removed by small translations of the cell.[70]

A number of different pathlengths were explored to maximize the fifth-order signal while keeping cascaded signals at an acceptable level to avoid contamination. A pathlength of 500 $\mu$m was found to be the best compromise. It should be noted here that the signal levels for this pathlength are very similar to that observed for $CS_2$ with 100 $\mu$m pathlength and gives the first indication that the theoretical predictions for the signal amplitude are correct to within factors of 2. The liquid was pumped by a peristaltic pump (Rabbit) to avoid excessive mechanical vibrations. All of the optics were placed in a covered box to reduce air current and improve the overall stability.

### B. Phase matching considerations

The DO used in these experiments has been described previously.[71,72] The main difference between this experiment and previous work is the longer pathlength. Here, we have to consider the relative contributions of the desired fifth-order nuclear response from undesired lower order cascades. The direct fifth-order Raman signal field $E_s(t)$, due to the induced fifth-order polarization from the five incoming pulses over a pathlength $l$, can be expressed as[70,75]

$$E_s^{(5)}(\tau_2,\tau_4) = i\frac{l\omega_s}{n_s}E_1E_2E_3E_4E_5R^{(5)}(\tau_2,\tau_4)F(\Delta k,l), \qquad (1)$$

where $F(\Delta k,l)=\sin(\Delta kl/2)\exp(i\Delta kl/2)/(\Delta kl/2)$ is the phase matching factor.

In addition, the cascaded third-order Raman can be written as

$$E^{(3)}_{nmllkji,\text{sequential}}(\tau_2,\tau_4) = -\left(\frac{l\omega}{n}\right)^2 E^5[R^{(3)}_{\alpha kji}(\tau_2)R^{(3)}_{nml\alpha}(\tau_4) \times F(\Delta k_{s1a},l)F(\Delta k_{s1b},l) + R^{(3)}_{\alpha lji}(\tau_2)R^{(3)}_{nmk\alpha}(\tau_4) \times F(\Delta k_{s2a},l)F(\Delta k_{s2b},l)], \qquad (2)$$

TABLE I. Phase matching parameters for the cross beam geometry in liquid formamide with a 500 $\mu$m sample length.

| Process | $\Delta k_a$ (cm$^{-1}$) | $\Delta k_b$ (cm$^{-1}$) | $\lvert F(\Delta k,l)\rvert$ |
|---|---|---|---|
| Direct | −20.2633 | | 0.9578 |
| Sequential 1 | 494.7593 | 470.0373 | 0.0010 |
| Sequential 2 | 435.7771 | 413.6343 | 0.0070 |
| Parallel 1 | 950.0701 | −961.8025 | 0.00152 |
| Parallel 2 | 950.0701 | 961.8024 | 0.00152 |

$$E^{(3)}_{nmllkji,\mathrm{parallel}}(\tau_2,\tau_4) = -\left(\frac{l\omega}{n}\right)^2 E^5[R^{(3)}_{\alpha mji}(\tau_2+\tau_4)R^{(3)}_{n\alpha lk}(\tau_4) \times F(\Delta k_{p1a},l)F(\Delta k_{p1b},l) + R^{(3)}_{\alpha mlk}(\tau_2+\tau_4)R^{(3)}_{n\alpha ji}(\tau_4) \times F(\Delta k_{p2a},l)F(\Delta k_{p2b},l)]. \quad (3)$$

These equations showed that the phase matching and sample pathlength are two key factors in deciding the amplitude of the scattered signal. For purely direct fifth-order Raman signal, the ideal phase matching conditions should maximize the phase matching for the direct fifth-order Raman response and simultaneously provide a significant phase mismatch for each step of the cascaded processes to reduce the overall cascaded third-order Raman contribution to the detected signal. As discussed previously, by taking advantage of DO's and spatial filters, it is possible to readily convert between two beam geometries with different degrees of contrast against cascaded third-order processes as a test for the relative signal contributions.[70–72] The beam geometry with the greatest discrimination is the crossed beam geometry where the angle between excitation pulse pairs is increased and correspondingly significantly increases the discrimination against cascades. This feature was additionally checked by using the Dutch Cross polarization condition for the six fields to ensure signal purity.[73]

Table I lists the calculated data for phase matching factors for the cross beam geometry for liquid formamide with the pathlength used. This table shows that the pure fifth-order Raman signal is well discriminated against lower order cascades. It should be noted that the third-order response is smaller in liquid formamide than in $CS_2$ to the same degree as the fifth-order response. The problem with respect to signal optimization scales well with increased pathlength for weaker fifth-order responses if the relative contributions scale in this manner. *A priori*, it was not known how the relative first-order polarizabilities, $\alpha^{(1)}$, scaled in relation to the critical nonlinear polarizability, $\alpha^{(2)}$ term. Based on the recent theoretical work,[82] it appears that the two are connected. This observation reflects that the relative shape of the $q$ dependent polarization is very similar for different systems; the larger the $\chi^{(3)}$ response is, the larger will be the $\chi^{(5)}$ response. This new insight provides a simple scaling relation, using $CS_2$ as a reference signal, that will provide sufficient guidance in experimental design in the study of other liquids.

### C. Hybrid molecular dynamics simulations

The fifth-order 2D Raman signals were commonly calculated from the equilibrium and nonequilibrium finite field MD simulations.[44–46,62,63,67–69] The equilibrium method evaluates response functions with equilibrium trajectories,[44–46,67–69] while the nonequilibrium method calculates a molecular polarizability from nonequilibrium trajectories[62,63] for different pulse configurations and sequences. In the present study, we use the hybrid approach, which combines the existing two methods to avoid the time-consuming calculations of the stability matrices which are inherent in the equilibrium method. The details of the simulation procedure were presented in Ref. 82. The conditions of the simulations were as follows. The simulation box was prepared with 64 rigid formamide molecules at 1 bar and 300 K, with the box length producing the density of 1.12 g/cm$^3$. To investigate the difference between the intermolecular potentials for formamide with respect to the signals, we employed two kinds of potentials, the modified T-model potential[87,88] and the optimized potential for liquid simulations (OPLS) potential.[84–86] The molecular polarizability was taken from Ref. 89 and was assumed to be in the center of the molecular mass. The equations of motion were solved by the velocity Verlet integrator of rigid bodies with the time step of 2.5 fs.[90,91] We first made 168 temporary configurations from a *NVT* (*N*, number-of particles; *V*, volume; and *T*, temperature) trajectory at 100 ps intervals. We then took fragments of 100 ps *NVE* (*N*, number of particles; *V*, volume; and *E*, energy) trajectory from the temporary configurations after 25 ps equilibration. The initial configuration of the nonequilibrium MD (NEMD) calculations was sampled at 5 fs intervals from each fragment of the trajectories. During the NEMD simulations, the response was calculated from the microcanonical ensemble with an electric field of $6\times10^{20}$ V/Å applied with $1.0\times10^{-40}$ fs time step, so that we used $E^2\Delta t=36$ (V/Å)$^2$ fs. To have reasonable signals against numerical noise, we averaged over $3\times10^6$ initial configurations for the fifth-order response function.

## III. RESULTS

### A. All parallel polarization: $R^{(5)}_{zzzzzz}$

Figure 2 shows the homodyne or direct signal detection for the all parallel polarization configuration. The polarizations for all the input pulses and detected signal were set to be parallel by using various polarizers and checked for consistency with an analyzer. The 2D datasets are obtained by scanning the $\tau_4$ stage (scan length is 1500 fs) with one data point per femtosecond, while keeping the $\tau_2$ stage fixed at some time delay point, then moving the $\tau_2$ stage to a new time delay with time increments of 50 fs. The $\tau_4$ stage is scanned for each $\tau_2$ with the process repeated until all the needed data are obtained. Note that it was not possible to use smaller $\tau_2$ steps as laser drift over time prohibited longer data collection times. As it was, this data set took over 2 h to acquire.

The results in Fig. 2 show that the highest signal occurs near the time zero point $\tau_4=\tau_2=0$. This signal is due to the

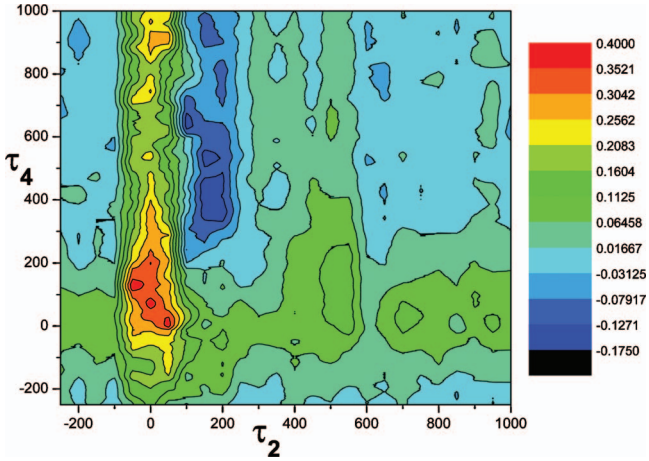


FIG. 2. (Color) Homodyne detected fifth-order Raman signal of formamide for the $R^{(5)}_{zzzzzz}$ tensor element.

instantaneous electronic hyperpolarizability term contributing to $\chi^{(5)}$. It is unrelated to the nuclear response. This signal effectively tracks the input pulse excitation and gives an indication of the time resolution along the various axes in the 2D spectrum. This signal contribution unfortunately obscures the first 100 fs of the signal response and makes it difficult to assign positions of nodal planes in the 2D spectrum that have been shown to be key indicators of the accuracy of the potential used in modeling the response.[80,82] However, the electronic response can be used as an internal reference for the relative signs of the different signal components, as will be discussed below. The most prominent feature that appears to be common to all fifth-order response functions as derived experimentally or theoretically is the strong focusing of the signal along the $\tau_4$ axis. The signal is stretched along this axis and decays with a 1/e on the order of 300 fs. This decay feature is much faster than the nuclear free induction decay observed in the lower order $\chi^{(3)}$ response[16,83–86] and illustrates the new information content at this order of field interaction. In stark contrast to the signal along $\tau_4$ ($\tau_2$=0 axis), there is only a pulse width limited decay along $\tau_2$ ($\tau_4$=0). This result is expected as there is no time for the accumulated nuclear response from the two excitation pulse sequences to accrue. Again, this signal dependence is expected and is different from previous reports where there was a strong signal along this axis.[75–77,79] As discussed above, more recent studies indicate that these earlier reports have some contributions from lower order cascades. In the homodyne detected 2D spectrum, the signal amplitude along the diagonal is too small to observe any semblance of an echo response.

The above is the signal intensity and is given by $|\chi^{(5)}|^2$. There are important details such as the nodal planes and sign of the signal that are lost in direct intensity detection. By beating this signal against a local oscillator, it is possible to detect the signal field directly. The signal is then proportional to $|\chi^{(5)}|$, in which case the signs and relative phase of the signal response are conserved. Also, one can amplify the signal by increasing the amplitude of the reference field. The experiment gains in sensitivity and information content if the signal can be detected through a cross term with a reference

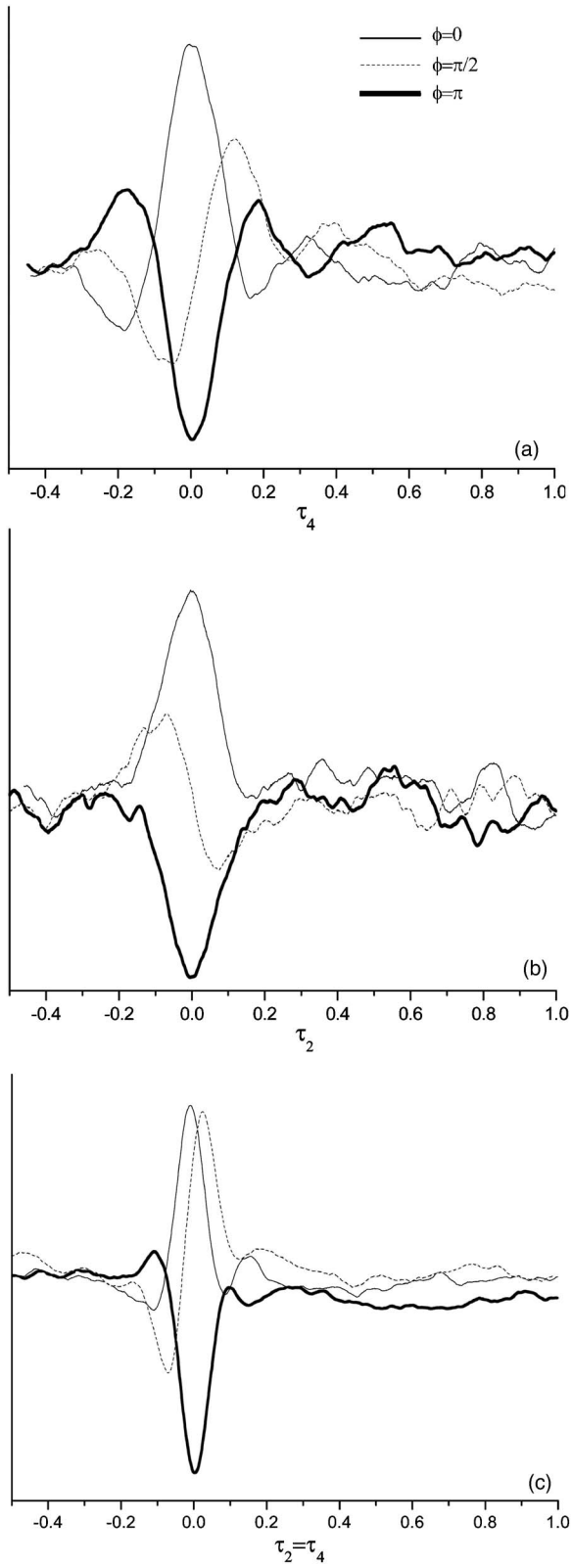


FIG. 3. Heterodyne detected fifth-order Raman response for $R^{(5)}_{zzzzzz}$ tensor element. (a) Time slice is along the probe delay ($\tau_2$=0 axis). (b) Time slice is along the excitation pulse delay ($\tau_4$=0 axis). (c) Time slice is along the diagonal ($\tau_2=\tau_4$), clearly showing rephasing at $\tau_2=\tau_4$=150 fs.

field in a process referred to as heterodyne detection in the time domain, even though the signal field and reference field are of the same central carrier frequency. These results are shown in Fig. 3, in which the small homodyne signal is

subtracted and measured response corrected for pump induced reference modulation as described previously.[70] Despite the high stability of the DO setup, it is not possible to prevent drift in the phase during the entire time needed to collect a 2D spectrum. The general features are given by the homodyne detected signal. Instead, the focus in the heterodyne detected experiments was on getting high quality time slices that could be quantitatively compared to theory. In this regard, Fig. 3(a) shows the heterodyne detected $\tau_4$ slice measured for different relative phase settings between the reference and signal fields for $R^{(5)}_{zzzzzz}$ ($\tau_2=0$ axis). The slice along the $\tau_2$ axis is shown in Fig. 3(b) ($\tau_4=0$ axis) and the diagonal slice ($\tau_2=\tau_4$) is shown in Fig. 3(c). It needs to be noted that the zero phase between the reference and the signal, corresponding to $\Delta\varphi=0$, is defined by the phase which maximizes signal intensity at $\tau_2=\tau_4=0$. This is not an absolute phase setting but it is useful, so that other phase scans along different axes have a common reference phase. Previously, we have shown that the 90° phase shifted data from this condition are dominated by the electronic hyperpolarizability and appear as a derivative of the excitation fields in analogy to the separation of Im and Re components of $\chi^{(3)}$ signals.[70] The small modulation in the $\Delta\varphi=0°$ and 180° relative phase settings before $t=0$ is due to incomplete separation of the in phase and out-of-phase signal fields. With the significantly smaller signals from liquid formamide relative to $CS_2$, it was not possible to do enough scans to better resolve the optimal phase setting.

The main features of the time slices shown in Fig. 3 are as follows: (1) The basic features of the in-phase scan along $\tau_4$, $\tau_2$, and diagonal are the complicated slow decay along $\tau_4$, the very fast clear decay along $\tau_2$, and the well-defined nuclear rephasing peak along the diagonal. For each phase setting for the $\tau_4$ scans ($\tau_2=0$ axis), there are two different times where the signal changes sign. The instantaneous electronic feature is pulse width limited and appears as a symmetric feature centered at $\tau_4=0$ for the in-phase ($\Delta\varphi=0°$) and out-of-phase ($\Delta\varphi=180°$) scans, although of opposite signs as expected. The 90° phase shifted scan shows the electronic hyperpolarizability as a derivative. This difference in nonlinear response of the electronic contribution has been seen before in $\chi^{(3)}$ experiments for heterodyne detection with 90° phase differences.[92] The subsequent response to the instantaneous electronic hyperpolarizability shows a sign change to the opposite signal plane for the in-phase and out-of-phase scans followed by a slow decay that is due to the nuclear response. The 90° phase shifted response shows an asymmetric shape around $\tau_4=0$ with enhanced signal showing up at positive delay times due to the contribution of the nuclear response. In comparing all the phase scans, there is a clearly discernable nuclear decay feature that has a peak amplitude at around 200 fs followed by a decay that is obscured by the noise in the signal. The slow decay has a 1/e of approximately 300 fs that is more readily observable in the homodyne detected signal (Fig. 2). This feature was observed in the many traces taken along this time slice. In comparing the signal amplitude of the long lived component to the instantaneous electronic response symmetrically disposed to the time origin, we observe that the nuclear response is opposite in sign to the electronic hyperpolarizability along this axis and will be discussed further below. (2) The response along the $\tau_2$ axis, as shown in Fig. 3(b) is clear. It is distributed nearly symmetrically with a full width at half maximum of 140 fs assuming a Gaussian shape. This observation is fully consistent with previous results, which show that there is no nuclear $\chi^{(5)}$ response along this axis. The signal along this axis is dominated by the electronic hyperpolarizability and is approximately pulse width limited. This feature is equally clear in the homodyne detected signal shown in Fig. 2. (3) The diagonal scan shown in Fig. 3(c) is the most revealing. Finally, we now observe an independent nuclear peak at $\tau_4=\tau_2=150$ fs that is clearly distinguishable. This signal component is a factor of 5 smaller than the electronic hyperpolarizability term and is consequently not discernable in the much smaller signal to noise in the homodyne detected signals. It is equally clear that the signal along the diagonal, the rephasing direction, has the same sign as the electronic hyperpolarizability. Therefore, there is a sign change in the nuclear response as one moves off axis from $\tau_2=0$ axis toward the diagonal $\tau_2=\tau_4$ axis. The exact position cannot be determined but can be estimated from the nodes in the slices shown in Figs. 3(a) and 3(c) to be around 100 fs.

### B. Dutch Cross response: $R^{(5)}_{l'l'zzll}$

The signal amplitude for the direct or homodyne detected fifth-order 2D Raman spectra is more favored by the all parallel excitation. The signal is decreased for other polarization tensors by the decrease in the vector projection of the induced polarization along the detected signal direction. Effectively, the field magnitude driving a given polarization anisotropy is reduced from the maximum that it could attain for all parallel polarizations of the input excitation fields. There have been predications for important differences in the different polarization tensor elements for $\chi^{(5)}$.[59,93] However, the differences are generally small and given the signal to noise limitations of the experiment, the differences are not pronounced enough to be informative. The greatest use of the different tensor elements is to help distinguish pure nuclear $\chi^{(5)}$ responses from cascades. In this respect, magic angle[93] detection of the signal offers advantages as collision induced polarization effects make a relatively larger contribution to the fifth-order than the third-order response and is of interest in its own right. However, to definitively distinguish between third-order and fifth-order processes, the best polarization configuration is to use 60° rotations between the two excitation pulse pairs and signal detection under which conditions, the third-order nuclear response cancels.[62] This polarization configuration, referred to as the Dutch Cross,[73] retrieves specifically the $\chi^{(5)}_{l'l'zzll}$ tensor element. The subscripts here refer to the relative polarization settings of the excitation pulse pairs and probe/reference pulse pair where the polarizations of the laser pulse excitation pairs are set relative to the horizontal plane along the $z$ axis (parallel with the optical table); $l$ denotes an angle of 60° counterclockwise of the $z$ propagation axis seen from the direction of the incoming laser beams for the first pumping laser pairs, and $l'$ denotes an angle of 60° clockwise for the probe and reference laser pairs.

In the Dutch Cross heterodyne detection, the intensity of the response is about one-fourth of the all parallel case. Furthermore, the pump induced modulation (PIM) of the reference is comparable to the all parallel case, such that there is an additional net reduction in the retrievable signal to noise by nearly an order of magnitude for this polarization configuration. In order to improve the signal, the data collection time and traces were increased as well as that for collection of the PIM scans. Many more scans and longer data acquisition times were required to isolate this signal component.

It was not possible to obtain reasonable quality homodyne detected signal for this beam geometry to make a full 2D scan. We can, however, report that the general trends are the same as observed in Fig. 2 in this respect. Heterodyne detection was essential to be able to discern the general features on any quantitative level. These results are shown in Fig. 4. Figure 4(a) shows the time slice along $\tau_4$ for different relative phase settings of the probe/reference pulse pair in heterodyne detection. The most distinguishing features from the all parallel data are the reduction in the electronic contribution to the signal and more pronounced nuclear response relative to the electronic signal. Again, the signal to noise is low for this tensor element but this feature is clear in all of the collected scans. The nuclear decay appears to be monotonic with a decay time of approximately 300 fs. This feature is significantly shorter than the free induction decay observed for liquid formamide at the $\chi^{(3)}$ level of response. Figure 4(b) shows the time slice along $\tau_2$ ($\tau_4=0$) and it clearly shows no semblance of a nuclear contribution. The fast decay along this direction is consistent with the observations for the all parallel case. Despite the poorer signal to noise, the signal from the Dutch Cross clearly illustrates the general features observed for the all parallel polarization tensor and demonstrates that this signal is free from significant cascades. The only main difference is that the nuclear and electronic hyperpolarizabilities appear to be of the same sign for this polarization configuration.

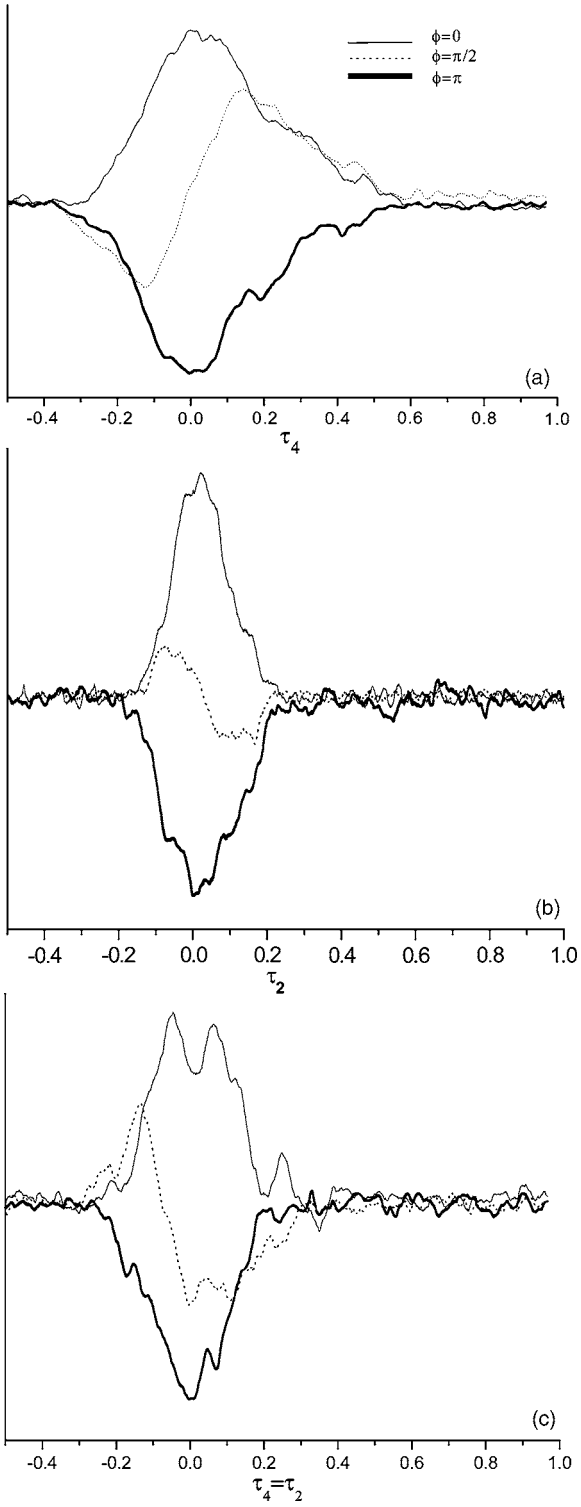


FIG. 4. Heterodyne detected fifth-order Raman response for the $R^{(5)}_{l'l'zzll}$ tensor element. The time slices are the same as in Fig. 3. The main features of the signal are conserved. The signal amplitude is reduced relative to the all parallel case as expected and illustrates the lack of significant lower order cascade contributions to the signal.

### C. MD calculations of the fifth-order response

The simulated results for the fifth-order Raman spectra have been calculated by using the equilibrium and nonequilibrium hybrid MD simulation algorithms, as discussed above. The final simulated 2D fifth-order Raman spectra and corresponding slices are presented in Fig. 5 for $R_{zzzzzz}$ and $R_{l'l'zzll}$ with the modified T-model [Figs. 5(A) and 5(B)] and OPLS potentials [Figs. 5(C) and 5(D)].[82,84–86] The difference between the 2D signal profiles for Figs. 5(A) and 5(C) is not prominent: Both figures exhibit positive peaks near the region of $\tau_4=\tau_2=100$ fs and negative ridges along the $\tau_4$ axis. The signal from the OPLS potential along $\tau_2$ shows a bit faster rise and decay than that from the modified T-model potential. The dynamics and structure on the OPLS and T-model potentials were discussed by Puhovski *et al.*[85,94,95] Note that the only difference between the T-model potential and the modified T model is the $R^{-6}$ coefficient of the dispersion and polarization terms. They concluded that the T potential offers a better description of formamide molecules than the OPLS potential. They also showed that the formamide molecules described by the OPLS potential made stronger hydrogen bonds, which exhibit faster vibrational motions than those described by the T-model potential. This tendency agrees with our simulation results. We observe a faster initial rise and oscillatory decay along the $\tau_4$ axis in the signals from OPLS shown in Figs. 5(C) and 5(D) than those from

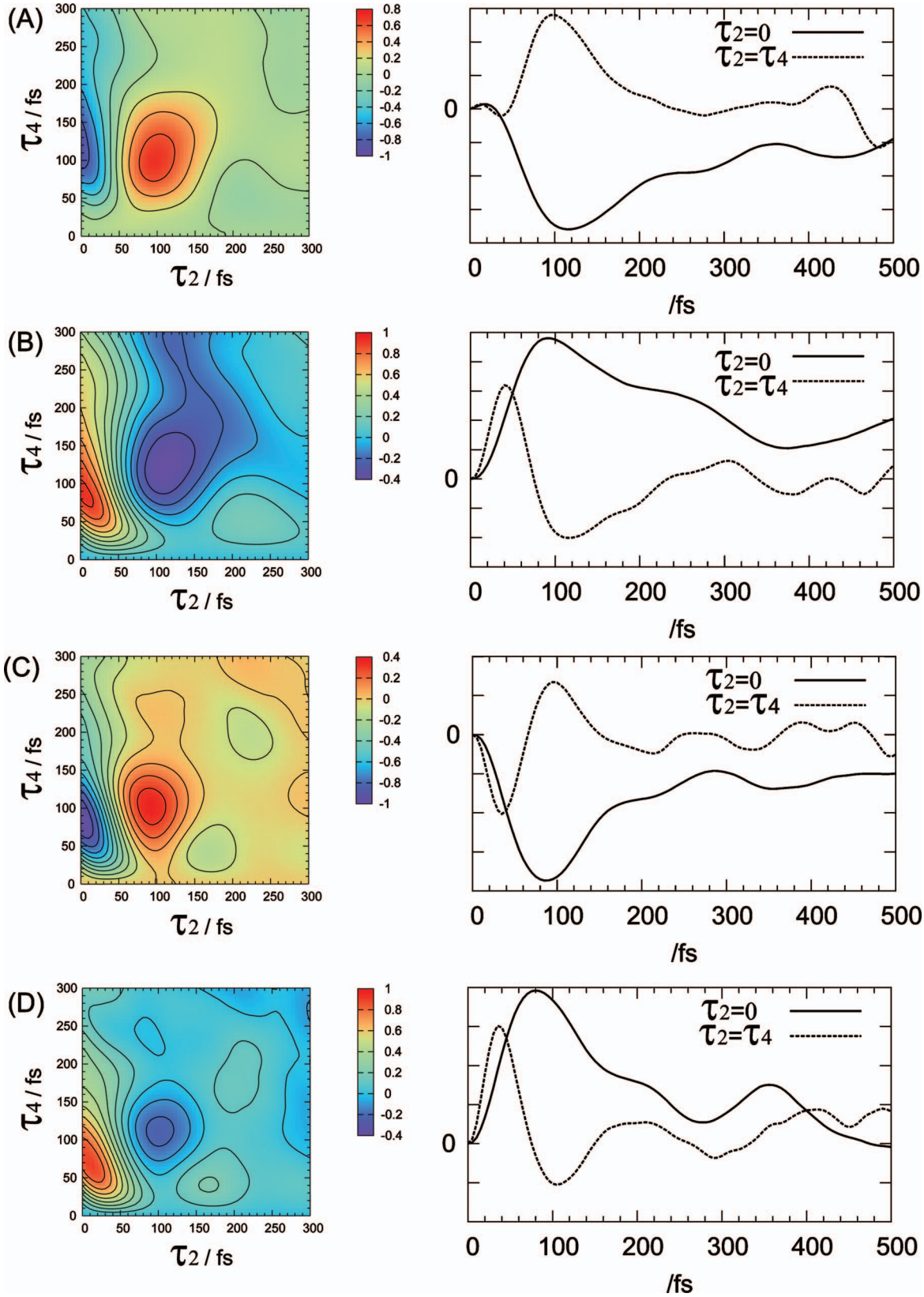


FIG. 5. (Color) MD calculations of the fifth-order response. (A) $R_{zzzzzz}$ with modified T potential. (B) $R_{l'l'zzll}$ with modified T potential. (C) $R_{zzzzzz}$ with OPLS potential. (D) $R_{l'l'zzll}$ with OPLS potential.

the modified T potential shown in Figs. 5(A) and 5(B). The decays of the signals are, however, not so clear due to the poor convergence of the signal on MD sampling trajectories for large $\tau_4$ and $\tau_2$. Qualitatively, the calculations agree with the experimental results, as will be discussed below. There are quantitative differences. Experimentally, there may still be small residual cascaded signal components not present in the simulated signals. Furthermore, the simulated signals do

not have the pure electronic and the electronic/nuclear signals, which may also contribute to the experimentally observed signals along the $\tau_2$ and $\tau_4$ axes. To include the pure electronic and the electronic/nuclear contributions, the second and the fourth molecular hyperpolarizabilities of formamide have to be evaluated. These values are difficult to obtain with reasonable accuracy. The lack of a signal along $\tau_2$ in the experiments indicates that the electronic-nuclear hyperpolarizability contribution is small but still could account for small differences through cross terms.

The fifth-order signals arise from the anharmonicity of the potential and the nonlinearity of the molecular polarizabilities. In the present simulations, we changed the form of the potential, while the molecular polarizabilities are fixed. It was shown that the 2D profiles of 2D Raman signals are more strongly affected by the molecular polarizability than the form of the potential.[96] Since conventional MD methods employ such material properties as the potential functions and polarizabilities in a rather empirical manner, the accuracy of the calculated signals is limited. To overcome this problem, one needs to carry out first principles MD simulations, although this method is not yet practical to calculate 2D signals at the current level of algorithm and CPU power.

With this consideration, the results show that most of the negative/positive responses are asymmetrically distributed along $\tau_4$ and can extend to 300 fs, and no sign changes can be found for the $\tau_4$ slices. As for the diagonal direction, there is an obvious peak in the nuclear signal seen near the region of $\tau_4=\tau_2=100$ fs with relative rapid dephasing along this rephasing pathway. The bath echo contribution is predicted to be very short lived for both model potentials. The OPLS potential relative to the T potential gives a faster response along $\tau_4$ and a faster decay along the diagonal decay; meanwhile, the Dutch Cross geometry leads to positive features that reduce the decay in the $\tau_2$ direction. The signal for the all parallel configuration is negative along the $\tau_4$ direction; a detailed analysis of this signal for $CS_2$ has shown that this feature indicates that the signal is dominated by vibrational anharmonicity.[44]

## V. DISCUSSION

Formamide is the simplest amide unit of the possible peptide linkages and also is a popular solvent for chemical reactions. There has been great interest in studying its properties as a model system for highly hydrogen bonded liquids and as the simplest system prior to the onset of covalently linked amide units that constitute protein chemistry.[16,83–86] The single formamide molecular unit is composed of a carbonyl group and an amino group that form hydrogen bonds similar to peptide linkages, which casts formamide as a strongly associated liquid. There are different views about the relative degree of hydrogen bonding and spatial arrangements of the hydrogen bonding in the liquid formamide structure that have come from x-ray diffraction, elastic neutron scattering, Raman/IR spectra, and a number of theoretical simulations.[84–86,97–100] Basically, two models have arisen as the best approximations of the liquid formamide structure. The first model is that there are cyclic dimers in which two nearest formamide molecules are bounded by the hydrogen bonds formed with NH group on the *cis* position. The second model is one evoking extended chain formation where the *trans* NH group of one molecule is connected to the C═O group of another molecule. For the early time dynamics, both of these descriptions can be used to capture some of the details of the structural correlations that dynamically interconvert. The question is what fraction of the liquid exists in these two limiting views of structure correlations? One can imagine that the actual distribution of hydrogen bonded configurations would be more complex than these two simple basis structures. Recent MD simulation have shown that the liquid is better depicted as a continuous rambling three-dimensional H-bond network with a wide variety of individual H-bond geometries, with a number of similarities with respect to dynamical fluctuations in hydrogen bond directed correlations to that of the dynamic structure of water.[101] In all cases, the relatively strong nature of the hydrogen bonds formed by different numbers of molecules and orientations leads to spatial correlations that greatly contribute to the large inhomogeneity that is peculiar to this liquid. At the same time, the hydrogen bonded network increases the anharmonicity in liquid systems, leading to very rapid energy redistribution and memory loss in the frequency correlations as observed recently for liquid $H_2O$ using 2D IR methods.[35–37] A comparable condition can prevail in liquid formamide for the N—H mode in N—H···O═C where the weakening of the N—H bond by hydrogen bonding should lower the energy of its $v=2$ state more than that of $v=1$ and lead to Fermi resonances that assist energy redistribution between the intramolecular and intermolecular degrees of freedom.[35,36,101] Thus, the high degree of spatial correlation imposed by the hydrogen bonding and the issue of energy redistribution with respect to fluctuations and dissipation among the spectral density of liquid modes bring great importance to the study of this liquid with fifth-order Raman detection. It is an ideal model system for bridging the effects of hydrogen bonding on the liquid structure and onset to more strongly correlated behavior in protein polypeptides.

To make the connection of the fifth-order Raman signal to the dynamic liquid structure, the issue of signal purity needs to be discussed. The weak direct fifth-order Raman signal is easily contaminated by the stronger third-order Raman signal through a two step cascade process. It is only with specific phase matching geometries that strongly select against both cascade steps that the true fifth-order response can be detected free of this artifact. This problem has plagued early attempts to attain 2D Raman signals and always needs to be considered. The third-order $\chi^{(3)}$ signal has a well-known response function, such that the cascaded process is equally well-defined. Calculations of the cascaded signal[70,75] showed that when the response is completely dominated by parallel cascades (two independent Raman scattering processes from the same modes), the signal will show a long ridge along $\tau_2$ and fast decay along $\tau_4$. If the signal is dominated by sequential cascades (two independent Raman scattering processes from different excited modes), the plots will be symmetrically distributed along both $\tau_2$ and

$\tau_4$. In contrast, the pure fifth-order nuclear $\chi^{(5)}$ response has no signal along $\tau_2$ or zero probe delay. Therefore, the signal components along $\tau_2$ can be used to assign the purity level of the fifth-order signal. From inspection of Fig. 2, there is no signal along $\tau_2$ ($\tau_4=0$) and indicates that the signal is dominated by the fifth-order nuclear response. In consideration of the $CS_2$ case study and the signals shown in Figs. 2 and 3, it is also apparent that the fifth-order electronic-nuclear hyperpolarizability contribution can be neglected as there is no significant signal along the $\tau_2$ axis.

To further check on the purity of the fifth-order signal from liquid formamide, we also did the control experiment with the Dutch Cross polarization configuration that removes cascades (Fig. 4). The signal level is approximately four to five times smaller relative to the all parallel case as expected for the different vector projections of the excitation fields. The relatively small change in absolute signal relative to the all parallel case illustrates that the signal does not arise from cascades. If it did, the signal would be reduced by several orders of magnitude. The signal is still rather small, such that it was not possible to collect a full 2D spectrum; only slices along the key directions in the 2D plot were possible. These single time slices are shown in Fig. 4 and capture the salient details of the 2D spectrum. Inspection of Fig. 4 shows that there is a nuclear response stretched along $\tau_4$ with no signal along $\tau_2$. The relatively long response time is due to the velocity mismatch between the two different colors used for the excitation and probe convolved over the 500 $\mu$m pathlength. In the previous work on $CS_2$, the pathlength was shorter and removed this limitation. Comparison of the all parallel configuration shows much more structure due to the interference between the larger electronic hyperpolarizability in relation to the nuclear contribution. The signal along the diagonal, $\tau_2=\tau_4$, is broadened and may show a small nuclear rephasing signal, but the signal to noise is too marginal with this configuration to clearly observe this signal contribution. The main point is that these results basically reproduce the general features of the all parallel signal shown in Figs. 2 and 3 and show that this signal is clearly free of cascades. Given the higher signal to noise of the all parallel configuration, we will confine most of the discussion to the all parallel polarization tensor component.

In comparing the experimental signal shown in Figs. 2 and 3 to the theoretical predictions (Fig. 5), the first important observation is the absolute magnitudes of the signal. With the hybrid MD method, it is possible to estimate the relative signal strengths of different liquids by taking advantage of the finite field strength used to perturb the liquid and quantify the response. By using this approach, it was estimated that the nuclear $\chi^{(5)}$ response of liquid formamide would only be down by one-fifth that of $CS_2$.[82] In comparing the heterodyne detected signal magnitudes for $CS_2$ with a 100 $\mu$m pathlength cell to the present results with a 500 $\mu$m cell, it is clear that the theoretical predictions have been borne out. In aligning our experiments by using liquid $CS_2$ under the same conditions, the signal from $CS_2$ is approximately ten times stronger. Given the various uncertainties in the potentials used for the two different liquids, this degree of agreement is excellent. The theory is able to quantitatively predict the signal levels, and this new feature will greatly augment our abilities to explore different liquids by using 2D Raman spectroscopy.

In comparing the different calculated 2D Raman spectra by using different potentials, one can see the sensitivity of the 2D spectrum to the intermolecular potential. Given that the same polarizability was used for the two potentials, the differences are more notable. At present, the experiments do not have sufficient signal to noise or time resolution to clearly extract these difference; however, moderate improvements in the laser technology will enable more detailed comparisons to theory. The qualitative features of the experiment are still sufficient to determine the relative accuracy of these two potentials in capturing the liquid dynamics. In this regard, the modified T potential is thought to better represent hydrophobic effects and preferential solution of ions. Both potentials predict a nuclear response along the $\tau_4$ axis that peaks at 100 fs and shows a rather rapid decay of approximately 200–300 fs in comparison with the much more extended nuclear response observed in the nuclear free induction decay of the third-order $\chi^{(3)}$ response. The signal in both cases is negative and indicates that the fifth-order Raman source term is dominated by vibrational anharmonicity (*vide infra*). The nuclear response in the experimental signal is difficult to discern along this axis as there are interferences with the electronic hyperpolarizability. It is clear from the 2D spectrum (Fig. 2) that the nuclear response is stretched along the $\tau_4$ axis as predicted, and from the heterodyne detected signals, for different phase settings, one can see a common feature that peaks between 100 and 150 fs and then rapidly decays as predicted. The sign of the nuclear $\chi^{(5)}$ response can be inferred by examining the finite response of the nuclear signal relative to the instantaneous response of the electronic hyperpolarizability. This latter contribution is readily recognized as the pulse width limited signal centered at the time origin ($\tau_4=0$; $\tau_2=0$). The nuclear signal along $\tau_4$ is opposite in sign to the electronic hyperpolarizability. This comparison gives a relative reference for comparing other nodal positions in the predicted 2D response. The most obvious marker in this case is that the nuclear rephasing along the diagonal, or motional echo, is predicted to be opposite in sign to the signal along $\tau_4$. This feature is seen. The different phase settings consistently find a nuclear response along the diagonal ($\tau_4=\tau_2$) that has the same sign of the instantaneous electronic hyperpolarizability signal, opposite to what is observed along the $\tau_4$ axis. This demonstrates that both the dynamics and the sign of the fifth-order response are accurately predicted by the hybrid MD method.

The relative sign of the nuclear response is important as it is related to the mechanism of the signal source term. For electronically nonresonant conditions as in the present case, the pure and direct fifth-order Raman response function can be expressed by[75]

$$R^{(5)}_{nmlkji} = \langle \xi_{nmlkji} \rangle \delta(\tau_2)\delta(\tau_2+\tau_4) + \frac{i}{4\hbar}\langle [\alpha_{nm}(\tau_4), \gamma_{lkji}(0)] \rangle \delta(\tau_2) + \frac{i}{2\hbar}\langle [\gamma_{nmlk}(0), \alpha_{ji}(\tau_4)] \rangle \delta(\tau_4) - \frac{i}{4\hbar^2}\langle [[\alpha_{nm}(\tau_2+\tau_4), \alpha_{lk}(\tau_2)], \alpha_{ji}(0)] \rangle. \quad (4)$$

The first three terms are related to the electronic or electronic/nuclear hyperpolarizability that was already discussed. The important term giving rise to the 2D spectrum is the last term that expresses the three-point polarizability correlation function of the liquid that leads to a rephasing process and removal of inhomogeneous contributions to the spectral response.

In Eq. (4), the polarizability can be expanded as[30]

$$\alpha(t) \cong \alpha^{(0)} + \alpha^{(1)}(q(t)-q(0)) + \tfrac{1}{2}\alpha^{(2)}(q(t)-q(0))(q'(t)-q'(0)) + \cdots . \quad (5)$$

Within such an expansion, the terms $\alpha^{(2)}$ and $\alpha^{(1)}$ refer to the second and first derivatives of the polarizability, respectively. The signal vanishes in the limit of a linear dependence of polarizability on coordinate. It is the second-order polarizabilty that gives information on the anharmonic liquid motions, but this will only be true if the source term comes from the nuclear motions and not second order $q$ dependent changes in the polarizability of the molecule itself. The two coupling terms to the field that lead to a fifth-order Raman signal arise form either (1) nonlinearity of the polarizability ($R^N$) on the vibrational coordinate by the intra- or intermolecular coupling or (2) the anharmonicity ($R^{\mathrm{An}}$) in the vibrational potential.[44–46,48,56] The nonlinearity contribution to the fifth-order Raman correlation function comes from two one-quantum transitions through the Raman interaction ($\alpha^{(1)}$) and one two-quantum transition derived from $\alpha^{(2)}$. According to the photon transition number changes, the nonlinearity of the polarizability is subtly divided into $R^{N1}$ and $R^{N2}$ to express the one-quantum transition and two/zero-quantum transition during time $\tau_2$, respectively.

So the fifth-order Raman response function can be rewritten as[45]

$$R^{(5)}_{efcdab}(\tau_2,\tau_4) \cong R^{N1}_{efcdab}(\tau_2,\tau_4) + R^{N2}_{efcdab}(\tau_2,\tau_4) + R^{\mathrm{An}}_{efcdab}(\tau_2,\tau_4). \quad (6)$$

The independent or mixed contributions to fifth-order Raman signal from the terms in Eq. (6) have already been explored in the MD studies of liquid $CS_2$. The results showed that the anharmonicity of the molecular vibrational modes and the nonlinearity of the polarizability are close in magnitude and both act to determine the response shape. Interference effects between the two lead to predicted nodes in the 2D spectrum.[44–46] The key feature is that the anharmonicity ($R^{\mathrm{An}}$) gives rise to a negative ridge distributed along $\tau_4$ that is confined in a narrow localized region at short $\tau_2$. This change in sign occurs at positions where the lower frequency, more anharmonic motions begin to dominate the signal. From an experimental standpoint, the relative magnitudes of the anharmonicity of the electronic polarizability and vibrational contributions to $\chi^{(5)}$ for $CS_2$ are not completely resolved. The temporal position along the $\tau_4$ axis has been predicted to occur at around 200 fs.[46] With the recent convergence of experimental results, the position of the nodal plane is less than 100 fs and indicates that vibrational anharmonicity effectively dominates for $CS_2$ for the dominant portion of the 2D spectrum. Higher time resolution and signal to noise are needed to definitely locate the nodal plane.

With respect to formamide, even within the limited signal to noise, it is clear that the nuclear signal along $\tau_4$ and the rephased nuclear signal along the diagonal $\tau_2=\tau_4$ are opposite in sign, in agreement with the theoretical predictions. In this regard, it has been shown that a negative feature along the $\tau_4$ axis ($\tau_2=0$) to the signal field is the signature of vibrational anharmonicity.[44,48] This prediction is based on the relative contributions of electronic nonlinear polarizability and vibrational anharmonicities. Given that the predicted absolute signal amplitude for formamide relative to $CS_2$ has been borne out experimentally and the relative signs along the $\tau_4$ axis and rephasing process along the diagonal are also consistent with experimental findings, we conclude that the fifth-order Raman signal is dominated by vibrational anharmonicity. This finding gives new insight into the anharmonic motions of hydrogen bond networks.

With the above caveat to the present understanding of $CS_2$, the apparent larger vibrational anharmonicity for formamide relative to $CS_2$ can be understood based on the stronger intermolecular forces involved in defining the liquid dynamics. The hydrogen bond between formamide molecules is an order of magnitude stronger than the weak van der Waals and interaction induced forces defining the liquid state of $CS_2$, whereas the electronic polarizability is smaller for formamide relative to $CS_2$. In this respect, the electronic polarizability and vibrational anharmonicity will not scale to the same degree with the increased amplitude in the attractive terms in the intermolecular potential for formamide relative to $CS_2$. Here, it should be noted that the original derivation of the fifth-order Raman response assumed level independent dephasing within a harmonic Brownian oscillator model for the bath. It is clear that the Raman overtones of liquid modes are nominally bound states and do not satisfy this condition. The decay in the rephasing along the diagonal is dominated both by polarization quenching[44] and damping of the overtones,[4,70] the very motion giving rise to the vibrational anharmonicity contributions to the nuclear $\chi^{(5)}$. The extensive hydrogen bonding in formamide leads to stronger intermolecular forces that better approximate a bound state or mode and thereby give rise to a larger vibrational anharmonicity contribution to the fifth-order Raman response than in $CS_2$. There are more modes that are not critically damped or overdamped that can contribute to the response of formamide compared to in the case of $CS_2$. Basically, the intermolecular forces are stronger in formamide and the anharmonic components will be correspondingly larger in relation to the electronic polarizability.

In this respect, the key feature in the experimental 2D spectrum is the clear observation of the nuclear rephasing

process along the diagonal for the all parallel configuration now for the first time. This feature was not observable for $CS_2$ and could only be clearly discerned for the Dutch Cross configuration[73] where the electronic contribution is suppressed. This feature in the experiment shows the more highly correlated nature of the hydrogen bonded character of liquid formamide in relation to $CS_2$ where the modal character is more rapidly lost.

It is along the rephasing direction that we can, in principle, distinguish between the two potentials. The predictions from the T potential show one maximum in the nuclear rephasing response, whereas the OPLS shows the rephasing changes sign with a node near 50 fs. Both potentials give similar predictions for an approximate 300 fs decay along $\tau_4$ as observed. The main difference is along the rephasing direction. The experimental signal along the diagonal does show narrowing of the electronic feature at the origin relative to other slices. This effect would arise if the nuclear signal was initially opposite in sign and would indicate that the OPLS potential is more accurate than the T potential. However, better signal to noise and time resolution will be needed to clearly make this distinction. The important result is that the calculated $\chi^{(5)}$ response is in very good agreement with respect to the predicted decays along the different axes and the signs of the signals, as well as absolute magnitudes. The degree of agreement can be considered to be excellent, taken in this context. There is a well-defined experimental signature along the diagonal in the 2D spectrum that will enable a direct experimental determination of the more accurate potential. Here the sensitivity and power of the fifth-order Raman experiment in probing the dynamic structure of liquids are made apparent.

At the present level of signal to noise, the key experimental feature is the clearly observable peak along the diagonal in the heterodyne detected signal. The signal is good enough and well separated to enable quantitative comparison to theory. Both the OPLS and T potential calculations predict that a maximum in the nuclear rephasing signal pathway should occur at $\tau_2=\tau_4=100$ fs. However, the experimental results place this maximum at approximately 150 fs. The electronic hyperpolarizability contribution complicates making a quantitative comparison, as the signal contribution from the electronic terms convolved to the finite pulse durations, can modify the location of expected features. To facilitate a direct comparison, Fig. 6 gives the calculated response, in which a pulse width limited electronic hyperpolarizability contribution, convolved to the pulse duration, is added to the signal. The center of the pulse is located at time 0 point, with a 60 fs Gaussian pulse duration.

The calculated response is compared directly to the observed signal along this direction. From this comparison, it is evident that the predicted peak position along the diagonal should be within the time resolution of the experiment and that the calculated response is significantly earlier in time than that observed. There is an important consideration with respect to laser excitation bandwidth in these experiments that has not been previously considered in this class of experiments. In order to excite all the relevant modes in a fifth-order Raman process, one must have twice the bandwidth of

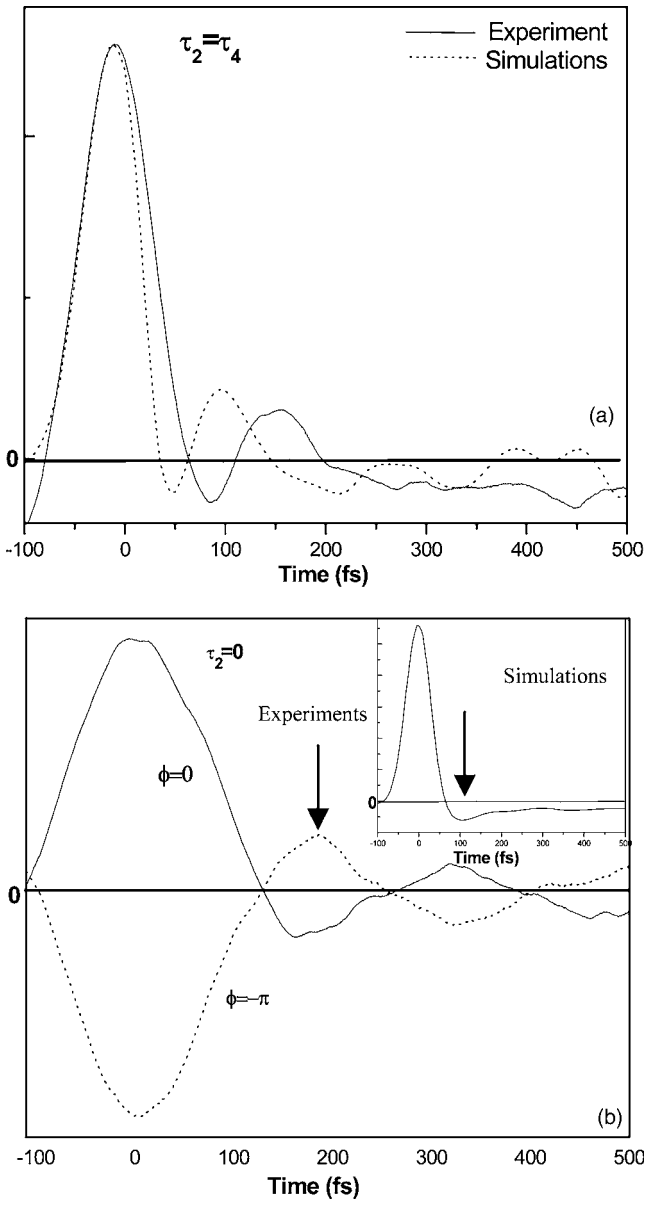


FIG. 6. Comparison between experimental and simulated total responses with the OPLS potential ($R_{\text{electronic}}+R_{\text{nuclear}}$) for (A) along the diagonal ($\tau_2=\tau_4$) and (B) along the probe delay ($\tau_2=0$). Note: The electronic contribution comes from the inclusion of a 60 fs Gaussian pulse duration.

the spectral density of states of the intermolecular spectrum as a two-quantum transition, or Raman overtone, is required for the rephasing process along this time slice. The theory uses an effective delta function excitation and excites all modes uniformly in this respect. The limited bandwidth of the laser in the experimental case biases the signal to the preferential excitation of lower frequency modes in relation to the simulation. This effect will lead to a delay in the nuclear rephasing pathway as it will be comprised of lower frequency components than that in the theoretical response. This detail likely explains the difference. We would also like to note that the OPLS also predicts a peak in the nuclear $\chi^{(3)}$ response that is faster than that observed experimentally,[16,83,86] so there appears to be some systematic deviations. In this respect, the observed fifth-order response now provides a good framework for refining the potential describing hydrogen bonded systems.

## VI. CONCLUSION

The fifth-order Raman response of liquid formamide has been experimentally resolved and shown to be free of significant lower order cascade contributions. The predicted signal level for liquid formamide relative to liquid $CS_2$ has been borne out experimentally. This finding alone is important as it demonstrates that the new hybrid MD finite field method can be used to facilitate the exploration of a number of different liquids and to correctly predict signal levels for guiding experiments. The equally important main features of the calculated response function have been born out as well. The 2D spectrum shows a strong focus along the $\tau_4$ ($\tau_2$=0) direction, with no signal along the $\tau_2$ axis ($\tau_4$=0). The decay along $\tau_4$ occurs with a 1/e time of approximately 300 fs. This feature was best resolved in the homodyne detected signals for the all parallel polarization configuration, as there seems to be some interference terms along this axis in the heterodyne detected signal. This approximate decay was also recovered in the Dutch Cross polarization configuration, in which any cascades are suppressed by several orders of magnitude. By using the sign of the electronic hyperpolarizability as a reference, the predicted signs of the signal are also shown to be correctly predicted and indicates that the signal is dominated by the vibrational anharmonicity in the many-body potential of liquid formamide. This result illustrates that the nuclear $\chi^{(5)}$ signal is sensitive to the details of the collective effects of the hydrogen bond network in liquid formamide. This distinction is most clearly seen in the rephasing direction along the diagonal, in which a very pronounced signal is observed that illustrates the much more structured nature of liquid formamide relative to simple liquids such as $CS_2$ with weaker intermolecular forces at play. Future experiments with higher time resolution will be able to clearly discern key differences in the predicted nodal positions for the different potentials used to model liquid formamide that provide information on anharmonic terms in both the intermolecular polarizability and vibrational anharmonicity. This work constitutes the first fifth-order Raman study of a hydrogen bonded liquid and represents an important step toward the ultimate goal of using the high sensitivity of the nuclear $\chi^{(5)}$ response to ultimately extending this approach to provide a rigorous potential for liquid water.

## ACKNOWLEDGMENTS

This work was supported by the Natural Sciences and Engineering Research Council of Canada and by the Japan Society for the Promotion of Science. R.J.D.M. would like to thank the Global COE Program for a fellowship during his stay at Kyoto University that facilitated this collaboration. T.H. is supported by the research fellowship of Global COE Program, International Center for Integrated Research, and Advanced Education in Material Science, Kyoto University.

[1] X. Shi, E. Borguet, A. N. Tarnovsky, and K. B. Eisenthal, Chem. Phys. **205**, 167 (1996).
[2] M. L. Horng, J. A. Gardecki, and M. Maroncelli, J. Phys. Chem. A **101**, 1030 (1997).
[3] S. P. Velsko, D. H. Waldeck, and G. R. Fleming, J. Chem. Phys. **78**, 249 (1983).
[4] K. J. Kubarych, C. J. Milne, and R. J. D. Miller, Int. Rev. Phys. Chem. **22**, 497 (2003).
[5] J. Z. Zhang, B. J. Schwartz, J. C. King, and C. B. Harris, J. Am. Chem. Soc. **114**, 10921 (1992).
[6] Y. L. Li, K. H. Leung, and D. L. Phillips, J. Phys. Chem. A **105**, 10621 (2001).
[7] M. Buchner, B. M. Ladanyi, and R. M. Stratt, J. Chem. Phys. **97**, 8522 (1992).
[8] K. Okumura and Y. Tanimura, J. Chem. Phys. **106**, 1687 (1997).
[9] O. Golonzka, M. Khalil, N. Demirdoven, and A. Tokmakoff, Phys. Rev. Lett. **86**, 2154 (2001).
[10] R. L. Murry, J. T. Fourkas, W. X. Li, and T. Keyes, J. Chem. Phys. **110**, 10410 (1999).
[11] R. L. Murry, J. T. Fourkas, W. X. Li, and T. Keyes, J. Chem. Phys. **110**, 10423 (1999).
[12] A. Ma and R. M. Stratt, Phys. Rev. Lett. **85**, 1004 (2000).
[13] T. Kato and Y. Tanimura, J. Chem. Phys. **117**, 6221 (2002).
[14] S. Palese, L. Schilling, R. J. D. Miller, P. R. Staver, and W. T. Lotshaw, J. Phys. Chem. **98**, 6308 (1994).
[15] M. C. Beard, G. M. Turner, and C. A. Schmuttenmaer, J. Phys. Chem. B **106**, 7146 (2002).
[16] Y. J. Chang and E. W. Castner, J. Chem. Phys. **99**, 113 (1993).
[17] N. A. Smith, S. J. Lin, S. R. Meech, H. Shirota, and K. Yoshihara, J. Phys. Chem. A **101**, 9578 (1997).
[18] M. Neelakandan, D. Pant, and E. L. Quitevis, J. Phys. Chem. A **101**, 2936 (1997).
[19] D. McMorrow and W. T. Lotshaw, J. Phys. Chem. **95**, 10395 (1991).
[20] M. C. Beard, W. T. Lotshaw, T. M. Korter, E. J. Heilweil, and D. McMorrow, J. Phys. Chem. A **108**, 9348 (2004).
[21] G. Hura, J. M. Sorenson, R. M. Glaeser, and T. Head-Gordon, J. Chem. Phys. **113**, 9140 (2000).
[22] A. H. Narten, J. Chem. Phys. **56**, 5681 (1972).
[23] A. H. Narten, J. Chem. Phys. **65**, 573 (1976).
[24] H. Bertagnolli, I. Waldner, K. Todheide, and A. K. Soper, Mol. Phys. **96**, 1075 (1999).
[25] T. Bausenwein, H. Bertagnolli, A. David, K. Goller, H. Zweier, K. Todheide, and P. Chieux, J. Chem. Phys. **101**, 672 (1994).
[26] R. F. Loring and S. Mukamel, J. Chem. Phys. **83**, 2116 (1985).
[27] Y. Tanimura and S. Mukamel, J. Chem. Phys. **99**, 9496 (1993).
[28] Y. Tanimura, J. Phys. Soc. Jpn. **75**, 082001 (2006).
[29] A. Ishizaki and Y. Tanimura, J. Phys. Chem. A **111**, 9269 (2007).
[30] T. Hasegawa and Y. Tanimura, J. Chem. Phys. **128**, 064511 (2008).
[31] P. Hamm, M. H. Lim, and R. M. Hochstrasser, J. Phys. Chem. B **102**, 6123 (1998).
[32] M. T. Zanni, M. C. Asplund, and R. M. Hochstrasser, J. Chem. Phys. **114**, 4579 (2001).
[33] H. S. Chung, Z. Ganim, K. C. Jones, and A. Tokmakoff, Proc. Natl. Acad. Sci. U.S.A. **36**, 14237 (2007).
[34] I. V. Rubtsov, K. Kumar, and R. M. Hochstrasser, Chem. Phys. Lett. **402**, 439 (2005).
[35] M. L. Cowan, B. D. Bruner, N. Huse, J. R. Dwyer, B. Chugh, E. T. J. Nibbering, T. Elsaesser, and R. J. D. Miller, Nature (London) **434**, 199 (2005).
[36] D. Kraemer, M. L. Cowan, A. Paarmann, N. Huse, E. T. J. Nibbering, T. Elsaesser, and R. J. D. Miller, Proc. Natl. Acad. Sci. U.S.A. **105**, 437 (2008).
[37] J. B. Asbury, T. Steinel, and M. D. Fayer, J. Phys. Chem. B **108**, 6544 (2004).
[38] J. Stenger, D. Madsen, P. Hamm, E. T. J. Nibbering, and T. Elsaesser, Phys. Rev. Lett. **87**, 027401 (2001).
[39] S. Sul, D. Karaiskaj, Y. Jiang, and N.-H. Ge, J. Phys. Chem. B **110**, 19891 (2006).
[40] T. J. Aartsma and D. A. Wiersma, Phys. Rev. Lett. **36**, 1360 (1976).
[41] L. J. Muller, D. Vandenbout, and M. Berg, J. Chem. Phys. **99**, 810 (1993).
[42] T. K. Yee and T. K. Gustafson, Phys. Rev. A **18**, 1597 (1978).
[43] K. Okumura and Y. Tanimura, J. Phys. Chem. A **107**, 8092 (2003).
[44] S. Saito and I. Ohmine, J. Chem. Phys. **108**, 240 (1998).
[45] S. Saito and I. Ohmine, J. Chem. Phys. **119**, 9073 (2003).
[46] S. Saito and I. Ohmine, Phys. Rev. Lett. **88**, 207401 (2002).
[47] K. Okumura and Y. Tanimura, Chem. Phys. Lett. **278**, 175 (1997).
[48] K. Okumura and Y. Tanimura, J. Chem. Phys. **107**, 2267 (1997).
[49] Y. Tanimura, Chem. Phys. **233**, 217 (1998).
[50] T. Steffen and Y. Tanimura, J. Phys. Soc. Jpn. **69**, 3115 (2000).

[51] T. Steffen and Y. Tanimura, J. Phys. Soc. Jpn. **76**, 078001 (2007).
[52] Y. Tanimura and T. Steffen, J. Phys. Soc. Jpn. **69**, 4095 (2000).
[53] T. Kato and Y. Tanimura, J. Chem. Phys. **12**, 260 (2004).
[54] M. H. Cho, J. Chem. Phys. **109**, 6227 (1998).
[55] A. Ma and R. M. Stratt, J. Chem. Phys. **116**, 4962 (2002).
[56] A. Ma and R. M. Stratt, J. Chem. Phys. **116**, 4972 (2002).
[57] J. S. Cao, S. L. Yang, and J. L. Wu, J. Chem. Phys. **116**, 3760 (2002).
[58] M. Kryvohuz and J. S. Cao, Phys. Rev. Lett. **96**, 030403 (2006).
[59] J. L. Wu, J. S. Cao, and J. T. Fourkas, J. Phys. Chem. A **111**, 9627 (2007).
[60] R. A. Denny and D. R. Reichman, Phys. Rev. E **63**, 065101 (2001).
[61] R. A. Denny and D. R. Reichman, J. Chem. Phys. **116**, 1987 (2002).
[62] T. L. C. Jansen, J. G. Snijders, and K. Duppen, J. Chem. Phys. **113**, 307 (2000).
[63] T. L. C. Jansen, J. G. Snijders, and K. Duppen, J. Chem. Phys. **114**, 10910 (2001).
[64] R. Devane, C. Ridley, B. Space, and T. Keyes, J. Chem. Phys. **119**, 6073 (2003).
[65] R. Devane, C. Ridley, B. Space, and T. Keyes, J. Chem. Phys. **123**, 194507 (2005).
[66] R. Devane, C. Ridley, B. Space, and T. Keyes, J. Chem. Phys. **125**, 234501 (2006).
[67] S. Saito and I. Ohmine, J. Chem. Phys. **125**, 084506 (2006).
[68] Y. Nagata and Y. Tanimura, J. Chem. Phys. **124**, 024508 (2006).
[69] Y. Nagata, T. Hasegawa, and Y. Tanimura, J. Chem. Phys. **124**, 194504 (2006).
[70] K. J. Kubarych, C. J. Milne, S. J. Lin, V. Astinov, and R. J. D. Miller, J. Chem. Phys. **116**, 2016 (2002).
[71] V. Astinov, K. J. Kubarych, C. J. Milne, and R. J. D. Miller, Opt. Lett. **25**, 853 (2000).
[72] V. Astinov, K. J. Kubarych, C. J. Milne, and R. J. D. Miller, Chem. Phys. Lett. **327**, 334 (2000).
[73] K. J. Kubarych, C. J. Milne, and R. J. D. Miller, Chem. Phys. Lett. **369**, 635 (2003).
[74] C. J. Milne, Y. L. Li, T. L. C. Jansen, and R. J. D. Miller, J. Phys. Chem. B **110**, 19867 (2006).
[75] D. A. Blank, L. J. Kaufman, and G. R. Fleming, J. Chem. Phys. **111**, 3105 (1999).
[76] D. A. Blank, L. J. Kaufman, and G. R. Fleming, J. Chem. Phys. **113**, 771 (2000).
[77] L. J. Kaufman, J. Y. Heo, L. D. Ziegler, and G. R. Fleming, Phys. Rev. Lett. **88**, 207402 (2002).
[78] Y. L. Li, L. Huang, and R. J. D. Miller (unpublished).
[79] L. J. Kaufman, S. Saito, L. D. Ziegler, I. Ohmine, and G. R. Fleming, *Ultrafast Phenomena*, edited by R. J. D. Miller, M. M. Murnane, N. F. Scherer, and A. M. Weiner (Springer, Berlin, 2003), Vol. 13, p. 554, Fig. 1.
[80] C. Milne, Y. L. Li, and R. J. D. Miller, *Time-resolved Spectroscopy in Complex Liquids*, edited by R. Torre (Springer, New York, 2007).
[81] S. Palese, J. T. Buontempo, L. Schilling, W. T. Lotshaw, Y. Tanimura, S. Mukamel, and R. J. D. Miller, J. Phys. Chem. **98**, 12466 (1994).
[82] T. Hasegawa and Y. Tanimura, J. Chem. Phys. **125**, 074512 (2006).
[83] Y. J. Chang and E. W. Castner, J. Phys. Chem. **98**, 9712 (1994).
[84] W. L. Jorgensen and C. J. Swenson, J. Am. Chem. Soc. **107**, 569 (1985).
[85] Y. P. Puhovski and B. M. Rode, Chem. Phys. **190**, 61 (1995).
[86] M. D. Elola and B. M. Ladanyi, J. Chem. Phys. **125**, 184506 (2006).
[87] K. P. Sagarik and R. Ahlrichs, J. Chem. Phys. **86**, 5117 (1987).
[88] M. C. Wojcik, K. Hermansson, and H. O. G. Siegbahn, J. Chem. Phys. **113**, 3374 (2000).
[89] J. Applequist, J. R. Carl, and K. K. Fung, J. Am. Chem. Soc. **94**, 2952 (1972).
[90] A. Dullweber, B. Leimkuhler, and R. McLachlan, J. Chem. Phys. **107**, 5840 (1997).
[91] G. Martyna, M. Tuckerman, D. Tobias, and M. Klein, Mol. Phys. **87**, 1117 (1996).
[92] G. D. Goodno, G. Dadusc, and R. J. D. Miller, J. Opt. Soc. Am. B **15**, 1791 (1998).
[93] R. L. Murry, J. T. Fourkas, and T. Keyes, J. Chem. Phys. **109**, 7913 (1998).
[94] Y. P. Puhovski, L. P. Safonova, and B. M. Rode, J. Mol. Liq. **103**, 15 (2003).
[95] Y. P. Puhovski, L. P. Safonova, and T. Suzuki, J. Chem. Soc., Faraday Trans. 2 **81**, 277 (1985).
[96] J. Ono, Y. Tanimura, and S. Saito (unpublished).
[97] R. J. Desando and G. H. Brown, J. Phys. Chem. **72**, 1088 (1968).
[98] F. J. Wiesmann, M. D. Zeidler, H. Bertagnolli, and P. Chieux, Mol. Phys. **57**, 275 (1986).
[99] O. F. Nielsen, P. A. Lund, and E. Praestgaard, J. Chem. Phys. **77**, 3878 (1982).
[100] K. Itoh and T. Shimanouchi, J. Mol. Spectrosc. **42**, 86 (1972).
[101] E. F. J. Nibbering and T. Elsaesser, Chem. Rev. (Washington, D.C.) **1041**, 1887 (2004).